05

Efficient generation of attopulses at the interaction of intense laser radiation with ultrathin targets

© A.A. Andreev[1,2], K.Yu. Platonov[3]¶

[1] St. Petersburg State University,
199034 St. Petersburg, Russia
[2] Ioffe Institute of RAS,
194021 St. Petersburg, Russia
[3] Peter the Great Saint-Petersburg Polytechnic University,
195251 St. Petersburg, Russia

¶ e-mail: konstantin_platonov@yahoo.com

Received April 28, 2021
Revised September 11, 2021
Accepted November 30, 2021

Parameters (thickness, electron density) of the laser target in the form of ultrathin foil are determined that provide maximum ($\sim 10\%$) conversion ratio of short relativistically intense laser pulses into a train of several coherent attopulses. Attopulse amplitude, duration are determined, conversion ratio of laser energy into the energy of attopulses is determined and the possibility of its increase using several successively located targets is shown.

Keywords: ultraintense laser pulse, attopulse, laser plasma, laser target.

DOI: 10.21883/EOS.2022.06.54713.2231-21

Introduction

A laser pulse of relativistic intense ($> 10^{18}$ W/cm^2) generates a current of relativistic electrons in the target, which, in turn, generate coherent and incoherent secondary radiation. This radiation is distributed over a wide interval of frequencies (from the initial optic range to gamma-quanta) and caused by a number of different physical mechanisms of its generation. For the potential use of the secondary radiation the important case is when many secondary harmonics of different frequencies in the spatial-time representation are put together in a train of ultrashort (10^{-18} s) attopulses [1]. These pulses are the only possible tool for instantaneous radiography and control of electron wave packets dynamics at subfemtosecond (subatomic) times [2], which makes it possible to investigate time dynamics and to control chemical and biological reactions. Attosecond pulses are resulted from the interaction of intense laser radiation with solid and gaseous targets and in the ideal case, they should have a close-to-rectangular frequency spectrum starting from the initial laser frequency up to the frequency corresponding to the inverse length of the attopulse. Consequently, among the possible physical mechanisms of secondary radiation generation we need to identify the mechanism to generate attopulses that results in the most low-sloped frequency spectrum of the radiation. The following mechanisms are known for the radiation of fast electrons at their relativistic oscillations in a thin target:

1. Transition radiation when electrons cross the plasma boundary. Radiation spectrum of a single electron [3] can be represented as a quasi-power spectrum with an power spectrum exponent of $q = -3/2$. Averaging over different (data calculated by the „particle-in-cell“ — PIC-method) energy distributions of fast electrons shows that spectral index of the transition radiation ($-q$) falls in the interval from 4/3 to 2 (the Maxwellian distribution yields $-q \sim 4/3$). Slope of the spectrum $\sim \omega^{-4/3}$ is low, however the transition radiation is incoherent in relation to the number of fast electrons and suppressed in relation to coherent mechanisms.

2. Braking radiation on target nuclei. It has a low-slope (independent on frequency, $q \sim 0$) spectrum, but is incoherent in relation to both the number of fast electrons and target nuclei. Consequently, the braking radiation is relevant for explanation of the „substrate“ of attopulses (the X-ray background), however it is ranked below coherent mechanisms in intensity.

3. Coherent „synchrotron“ emission (CSE) [4] of electron bunches in the skin-layer of laser plasma. CSE is responsible for the spectrum of radiation reflected from the plasma and coherent in relation to the number of fast electrons that makes it the main channel of the secondary radiation in terms of power. The CSE spectrum is of power-type $\sim \omega^{-4/3}$ [4], just as the spectrum of transition radiation, but CSE intensity is greater than that of transition radiation by a factor equal to the number of electrons in the bunch (i.e. by several orders of magnitude). Note, that in earlier models of CSE electron bunches were „replaced“ by a single relativistically oscillating plasma boundary [5], which resulted in a stronger drop of spectrum $\sim \omega^{-8/3}$. Since CSE is the main coherent channel of the secondary radiation, attopulses formed by the CSE mechanism have maximum

intensity, and the laser pulse is efficiently converted into a train of attopulses.

In this study the CSE is considered for the case of thin (units of nanometers) target near the transparency threshold. It is known that in this case [6] the energy of fast electrons oscillation increases as compared to the case of thick targets. This allows achievement of higher ratio of laser radiation conversion into train of attopulses. In contrast to the case of CSE in a thick target considered before [4,7], where attopulse spectrum asymptotics was analytically considered in the region of high frequencies (much higher than the laser frequency), in the case of thin target it turns to be possible to build up full spectrum of the reflected and passed through the target radiation. As a result, the conversion is determined more accurately than in [7], where full spectrum was replaced by its high-frequency asymptotics in the whole frequency range. In the region of high frequencies the power spectrum exponent of the thin target attopulse spectrum is in line with [7,8]. In addition to refining the intensity of low spectral harmonics affecting (defining) the conversion, in this work we optimized the target thickness providing maximum conversion ratio to attopulse at a given laser intensity. A formula for optimum target thickness as a function of incident intensity is derived. It is shown that in the optimum case the ratio of conversion to the attopulses propagating in the direction of the incident radiation is less than to the attopulses of the mirror direction. An explanation of this phenomenon by the asymmetry (forward-backward) of electron oscillations in the target within the field of laser pulse is given. To verify the analytical calculations, 1D and 2D PIC-modelling of attopulse spectra and values of the conversion ratio is carried out that confirms the quantitative relationships of the model. It should be noted that the numerical modelling of [9] demonstrated the emergence of a single attopulse in case of laser radiation reflection from the thin target. However, the absence of analytical model in this work and calculations with non-optimum parameters of the laser pulse and target resulted in low conversion ratios. In [10,11] methods of numerical modelling were used to select the target thickness in order to achieve maximum conversion ratio at given parameters of the laser pulse, but there were no analytical model and physical explanation of the obtained results. The suggested work is a further development of the ideas of [7–11] in order to build up an analytical model of attopulse generation by a single or several laser targets and to improve, on the basis of the model conclusions, the ratio of conversion of the laser pulse with given intensity and length into a train of attopulses.

The dynamics of electrons in a plasma target of finite thickness

Let us consider the incidence of a linearly polarized laser pulse onto a plasma layer of a finite thickness (the target).

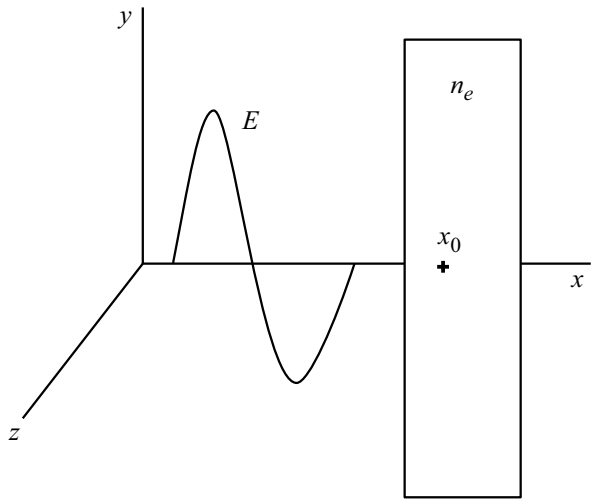

Figure 1. The geometry of interaction between the laser pulse and the target.

Assume the plasma layer consisting of a set of infinitely thin electron and ion layers. We neglect the motion of ions, assuming the length of laser pulse short as compared with the inverse ion plasma frequency. We assume laser beam diameter greater than the plasma layer thickness and consider the problem in a one-dimensional approximation. Assume x axis is normal to the target, y axis is along the direction of pulse polarization vector as shown in Fig. 1.

Let use write the equation for target electron dynamics in self-consistent electromagnetic fields. One-dimensional definition of the problem allows single integration over initial distribution of charges in Lienard-Wiechert potentials, determination of electromagnetic fields of the layer using the laws of electron motion and, as a result, writing dynamic equations containing only the external field, velocities and coordinates of electrons.

Electromagnetic field components of a plasma layer with initial profile of particle density $n_e(x_0) = Zn_i(x_0)$ are determined using the Green function of one-dimensional wave equation:

$$E_x(x,t) = -2\pi e \int_{-\infty}^{\infty} n_e(x_0)\,\mathrm{sign}\,(x - s(t', x_0))dx_0 + 2\pi e \int_{-\infty}^{\infty} n_i(x_0)\,\mathrm{sign}\,(x - x_0)dx_0,$$

$$E_y(x,t) = -2\pi e \int_{-\infty}^{\infty} n_e(x_0)\,\frac{v_y(t', x_0)/c}{1 - \mathrm{sign}\,(x - s(t', x_0))\dot{s}(t', x_0)/c}\,dx_0 - \frac{\partial A_y^{(\mathrm{ext})}(x,t)}{c\partial t}, \quad (1)$$

$$H_z(x,t) = -2\pi e \int_{-\infty}^{\infty} n_e(x_0) \frac{\mathrm{sign}(x - s(t', x)) v_y(t', x_0)/c}{1 - \mathrm{sign}\,(x - s(t', x_0))\dot{s}(t', x_0)/c}\, dx_0 - \frac{\partial A_y^{(\mathrm{ext})}(x,t)}{\partial x},$$

In (1) $s(t, x_0)$ — motion law of infinitely thin electron layer with initial coordinate x_0, $A_{x,y}^{(\mathrm{ext})}(x,t)$ — vector potential of the external (laser) field, $v_{x,y}(t, x_0)$ — projections of electron velocity in the thin layer with initial coordinate x_0. Retarded time $t'(x, x_0, t)$ in (1) is determined from the retardation equation:

$$t - t' - \frac{|x - s(t', x_0)|}{c} = 0.$$

Target thickness l_f is included as a parameter in the initial profile of target density $n_i(x_0)$.

Motion laws $s(t, x_0)$, $v_{x,y}(t, x_0)$ are determined from the motion equations where fields (1) are taken in the location of the electron layer $x = s(t, x_0)$, which is resulted in an integro-differential equation for $s(t, x_0)$ and $v_y(t, x_0)$ functions:

$$\begin{aligned}
\frac{d}{dt} & \frac{m_e v_y(t, x_0)}{\sqrt{1 - v_y^2/c^2 - \dot{s}^2(t, x_0)/c^2}} = -2\pi e^2 \int_{-\infty}^{\infty} n_e(x_0') \\
& \times \frac{v_y(t', x_0')/c}{1 - \mathrm{sign}\,(s(t, x_0) - s(t', x_0'))\dot{s}(t', x_0')/c}\, dx_0' \\
& - \frac{\partial e A_y^{(\mathrm{ext})}(s(t, x_0), t)}{c\partial t} + \frac{2\pi e^2 \dot{s}(t, x_0)}{c} \int_{-\infty}^{\infty} n_e(x_0') \\
& \times \frac{\mathrm{sign}\,(s(t, x_0) - s(t', x_0'))v_y(t', x_0')/c}{1 - \mathrm{sign}\,(s(t, x_0) - s(t', x_0'))\dot{s}(t', x_0')/c}\, dx_0' \\
& - \frac{\dot{s}(t, x_0)}{c} \frac{\partial e A_y^{(\mathrm{ext})}(s(t, x_0), t)}{\partial x}, \\
\frac{d}{dt} & \frac{m_e \dot{s}(t, x_0)}{\sqrt{1 - v_y^2/c^2 - \dot{s}^2(t, x_0)/c^2}} \\
& = -2\pi e^2 \int_{-\infty}^{\infty} n_e(x_0')\, \mathrm{sign}\,(s(t, x_0) - s(t', x_0'))dx_0' \\
& + 2\pi e^2 \int_{-\infty}^{\infty} n_i(x_0')\mathrm{sign}\,(s(t, x_0) - x_0')dx_0' \\
& - \frac{2\pi e^2 v_y(t, x_0)}{c} \int_{-\infty}^{\infty} n_e(x_0') \\
& \times \frac{\mathrm{sign}\,(s(t, x_0) - s(t', x_0'))v_y(t', x_0')/c}{1 - \mathrm{sign}\,(s(t, x_0) - s(t', x_0'))\dot{s}(t', x_0')/c}\, dx_0' \\
& + \frac{v_y(t, x_0)}{c} \frac{\partial e A_y^{(\mathrm{ext})}(s(t, x_0), t)}{\partial x}, \qquad (2)
\end{aligned}$$

The retardation equation in system (2) is as follows

$$t - t' - \frac{|s(t, x_0) - s(t', x_0')|}{c} = 0 \qquad (3)$$

and yields the dependence of retarded time $t'(x_0, x_0', t)$. Terms of sum with integrals over dx_0' in system (2) describe the effect of thin electron layers of the target on each other (self-action). Note that if the integrals are approximated by sums, system (2) is equivalent to equations for dynamics of fields and quasiparticles of collisionless 1D PIC-code. Equations of system (2) describe the following physical processes:

The second (lower) equation describes nonlinear oscillations $s(t, x_0)$ of the thin electron layer under the action of the ponderomotive pressure force of the external field (the last term in the sum in the right part), the ponderomotive pressure force of the layer scattered by the target (the third term in the sum), the force of longitudinal ambipolar (Coulomb) field of ions (the second term in the sum) and the force of longitudinal ambipolar field of neighboring electron layers (the first term in the sum in the right part). The ambipolar field of ions has a structure of potential well where nonlinear oscillations of the electron layer take place under the action of ponderomotive pressure force.

The first equation of the system is an equation for the transverse velocity of electrons, in terms of which, according to (1), the scattered transverse field is expressed, and therefore it is equivalent to an equation for the field scattered by the target. The attopulse of the scattered field arises due to longitudinal relativistic oscillations of electron layers in the target. The motion with near-light speeds results, due to the Doppler effect, in emergence of high-frequency harmonics of the scattered radiation corresponding to the emergence of attosecond pulses. The ratio of laser radiation conversion into attopulses is defined by the amplitude $s(t, x_0)$ and speed $\dot{s}(t, x_0)$ of the longitudinal nonlinear oscillations. The conversion reaches its maximum at the nonlinear resonance between the driving force of ponderomotive pressure and self-oscillations of electrons in the field of ion core. Consequently, the main purpose of this study is to determine the parameters to realize the nonlinear resonance and to determine the conversion ratio corresponding to this resonance.

System (2) is simplified in the extreme cases of thick ($l_f \gg l_s$) and thin ($l_{f<l_s}$) target, where l_s is thickness of skin layers. The case of semi-infinite $l_f \to \infty$ target is considered in [9]. In this extreme case it is sufficient to consider the motion (oscillations) of electrons in the skin layer on the target front side of the target. The transverse field in this case is a standing wave in vacuum and exponentially decays in the plasma. The potential of ions near the boundary is approximated by a parabolic potential (harmonic oscillator). Spectral intensity of the secondary radiation in this model is determined in [12]. The efficiency of conversion into attopulse in this case is far from its maximum possible value [7,8], because the semi-infinite plasma significantly screens the laser field on its surface.

The case of thin (less than or an order of skin layer thickness) target was considered in [13], however, in [13] the effect of target ion core field on the motion of electron layer was not taken into account. As it is shown in the following text, the resonance between forces of the ambipolar field and ponderomotive pressure significantly increases the attopulse intensity, therefore the calculation of attopulse parameters and conversion ratio taking into account the effect of ion field is a relevant task and a further development of [13]. Physical cause of the increase in conversion efficiency of thin target is its lower screening effect on the laser field, which increases the energy and current of fast electrons and the secondary radiation intensity, respectively. Note that the approximation of thin target assumes that there is no pre-pulse before the main pulse, and a steep leading edge (super-Gaussian longitudinal profile) of the main pulse. Currently, a high contrast (suppression of the pre-pulse) is obtained through the use of the „plasma mirror"technique, and methods to improve the leading edge steep are considered in [14]. When high-contrast pulses with a steep leading edge are used, a thin target can not break fast enough to a sufficient degree within the time interval of the first several laser cycles, and the following solutions to system (2) are correct.

In the extreme case of infinitely thin target, the motion laws $s(t, x_0)$ and $v_y(t, x_0)$ in (2) can be considered independent on the initial coordinate (all electron layers of the target move equally and $x_0 = 0$ for all layers). Then integrals in (2) can be calculated:

$$e\int_{-\infty}^{\infty} n_e(x_0)dx_0 = en_e l_f = \sigma_e, \tag{4}$$

which results in dependence of solution to (2) on the dimensionless parameter $\varepsilon_0 = \pi n_e l_f / n_\sigma \lambda$, and not separately from the density n_e and thickness l_f of the plasma layer. In the approximation of thin layer in (2) the retardation is insignificant as well: $t'(x_0 = 0, x_0' = 0, t) = t$. So, we get $\mathrm{sign}(s(t, x_0 = 0) - s(t', x_0')) = 0$, and thus, in the second equation of (2), the force of ambipolar field of neighboring electron layers and ponderomotive pressure of the scattered radiation disappears. The integro-differential equations (2) become differential equations in full derivatives and allow solution and analysis. In our previous work [15] these differential equations were used as a basis to consider the dynamics of thin target, but the spectrum of scattered radiation was not calculated.

An opposite extreme case is the case of thick target but not the semi-infinite target [12]. The difference from the model of [12] in this case consists in the presence of two target boundaries instead of one boundary. Numerical analysis of such targets using PIC-modelling shows that an increase in target thickness leads to weakening and degradation of the attopulse. Therefore in the following text an investigation of attopulse parameters for the extreme case of thin target is provided and conditions are found that make it possible to neglect the target blooming and attopulse degradation.

The analytical model of attopulse generation in a thin target

To solve system (2) for the extreme case of thin target, it is convenient to introduce the following dimensionless variables

$$a = |e|A_y/m_e c^2, \quad \tau = \omega t,$$
$$v_y(\tau, x_0 = 0)/c = u_y(\tau), \quad \omega s(\tau, x_0 = 0)/c = X(\tau),$$
$$\varepsilon_0 = \pi n_e l_f / n_{cr}\lambda = \omega_p^2 l_f / 2\omega c, \quad \theta = \tau - X,$$

where ω — frequency of the laser radiation, new unknown functions

$$p = \frac{u_y}{\sqrt{1 - u_y^2 - \dot{X}^2}}, \tag{5}$$
$$\Gamma = \frac{1 - \dot{X}}{\sqrt{1 - u_y^2 - \dot{X}^2}}$$

and a new argument $\theta = \tau - X$, which is a phase of incident electromagnetic wave. Functions (5) correspond to conservation laws of single ($\varepsilon_0 = 0$) electron in the field of traveling laser wave: $\Gamma = \mathrm{const}$, $P = p - a_y^{(\mathrm{ext})(\theta)=\mathrm{const}}$ at $\varepsilon_0 = 0$. In variables (5) equations of motion (2) in the approximation of layer with a thickness of ε_0 can be written as follows:

$$\Gamma \frac{dp}{d\theta} = -\varepsilon_0 p + \Gamma \frac{da_y^{(\mathrm{ext})}(\theta)}{d\theta},$$
$$(\Gamma^2 + p^2 + 1)\left(\frac{d\Gamma}{d\theta} + \varepsilon_0 f_{\mathrm{am}}(X)\right) = -2\varepsilon_0 p^2, \tag{6}$$
$$2\Gamma^2 \frac{dX}{d\theta} = 1 + p^2 - \Gamma^2,$$

where $a_y^{(\mathrm{ext})}(\theta) = a_0 \sin(\theta)\exp(-(\theta)^4/2(\omega t_L)^4)$ — amplitude of incident super-Gaussian laser pulse,

$$f_{\mathrm{am}}(X) = \begin{cases} -X2c/\omega l_f, & |X| < \omega l_f/2c, \\ -\mathrm{sign}\,(X), & |X| > \omega l_f/2c \end{cases} \tag{7}$$

— force of the ambipolar field between electron and ion layers. The potential corresponding to force (7) of the ambipolar field between thin layers of electrons and ions has the form of potential well, which is a parabola (if the offset of the electron layer does not exceed half thickness of the ion layer) with branches changing to inclined straight lines when the ion and electron layers become separated by a vacuum gap $|X(\theta)| > \omega l_f/2c$. Equations (6) are more convenient for solution than the equations in [15], because they do not contain relativistic roots and are polynomials of a degree not more than three in unknown functions and their derivatives. In particular, the expansion of system (6) in harmonics of laser frequency is performed in a more simple way than expansion of the initial system in [15].

Also, an important difference between equations (6) and those of [13] should be noted, i.e. the presence of two frequencies of nonlinear oscillations: the laser frequency (a fixed value) and the frequency of nonlinear oscillations of electrons in the ambipolar field (7) of ions (this frequency depends on amplitude of oscillations). In [13] there is no the second frequency, and equations (6) are considered in the approximation of $X = 0$, $\dot{X} = 0$ (there are no longitudinal oscillations of the electron layer). As a result, solution to (6) in [13] can be represented as a series in only odd harmonics of laser frequency, and spectrum of the secondary radiation is also composed of a set of odd harmonics. As shown in the following text, longitudinal oscillations of electron layer are considerable, they can be relativistic (dimensionless speed $\dot{X} \sim 1$) and yield even harmonics (harmonics of ponderomotive force), not taken into consideration in [13]. Since the longitudinal oscillations of the electron layer in the ambipolar field of ions have their own frequency, two incommensurable frequencies in general yield aperiodic solutions to (6) and a quasicontinuous spectrum of radiation. The most important issue for investigation is the nonlinear resonance between oscillations of the ponderomotive pressure force with double laser frequency and the frequency of longitudinal oscillations of electron layer in the potential well of the ion core. The longitudinal velocity at resonance is equal to its maximum value, which results in a maximum Doppler drift of the secondary radiation and generation of the highest frequencies among those of the attopulse spectrum.

Thus, to obtain parameters (including those of the spectrum) of attopulses, it is necessary to solve system (6), determine components of the transverse electromagnetic field of the target by formulae (1) in the thin layer approximation, and analyze them, including the investigation of their Fourier spectrum.

System (6) has no analytical solution for arbitrary values of two external parameters a_0, ε_0 and is integrated numerically. However, it is possible to find analytical solutions to (6) for the following two extreme cases: $a_0 < 1$ and $\varepsilon_0 < 1$. At $a_0 < 1$ and arbitrary ε_0 (nonrelativistic velocities of motion, low shift of the electron layer, absence of attopulse) solution to (6) is as follows:

$$u_y(\tau) = \frac{a_0}{1+\varepsilon_0^2}\sin\tau + \frac{\varepsilon a_0}{1+\varepsilon_0^2}(\cos\tau - e^{-\varepsilon_0\tau}),$$

$$X(\tau) = \frac{\varepsilon_0 a_0^2}{2(1+\varepsilon_0^2)\Omega^2}(1-\cos\Omega\tau) + \frac{a_0^2}{2(1+\varepsilon_0^2)(\Omega^2-4)}\sin 2\tau + \frac{\varepsilon_0 a_0^2}{2(1+\varepsilon_0^2)(\Omega^2-4)}(\cos 2\tau - \cos\Omega\tau),$$

$$\Omega^2 = \omega_p^2/\omega^2, \quad |X(\tau)| \le \omega l_f/2c. \tag{8}$$

It can be seen from (8), that at $a_0 < 1$ transverse oscillations occur at the first harmonic (at odd harmonics if further expanded), while longitudinal oscillations occur at the second harmonic (at even harmonics if further expanded). Also, it can be seen that longitudinal oscillations of the electron layer are excited at two independent frequencies: plasma frequency (Ω in (8)) and double laser frequency („2“ in (8) in arguments of trigonometric functions). At $\Omega = 2$ a resonance takes place between the frequencies — build-up of longitudinal layer oscillations. At $\varepsilon_0 < 1$ (target thickness tends to zero) an analytical solution can be obtained at arbitrary a_0:

$$p(\theta) = a_0\sin\theta + \varepsilon_0 a_0(\cos\theta - e^{-\varepsilon_0\theta}),$$

$$\Gamma(\theta) = 1 - \varepsilon_0\int\frac{2a_0^2\sin^2\theta}{2+a_0^2\sin^2\theta}d\theta + \frac{\Omega^2 a_0^2}{4}\int(\theta - (1/2)\sin 2\theta)d\theta = 1 - 2\varepsilon_0\theta + \varepsilon_0 2\sqrt{2}\frac{\operatorname{arctg}(\operatorname{tg}\theta\sqrt{1+a_0^2/2})}{\sqrt{2+a_0^2}} + \frac{\Omega^2 a_0^2}{8}\left(\theta^2 + \frac{\cos 2\theta}{2}\right),$$

$$\dot{X}(\theta) = \frac{1+p^2(\theta)-\Gamma^2(\theta)}{1+p^2(\theta)+\Gamma^2(\theta)}, \quad u_y(\theta) = \frac{2p(\theta)\Gamma(\theta)}{1+p^2(\theta)+\Gamma^2(\theta)}, \tag{9}$$

Solution to (9) at $a_0 \gg 1$ describes the electron layer flying away from the ion core, oscillating transversally and longitudinally at velocities of:

$$\dot{X}(\theta) \approx \frac{a_0^2\sin^2\theta}{2+a_0^2\sin^2\theta}, \tag{10}$$

$$u_y(\theta) \approx \frac{2a_0\sin\theta}{2+a_0^2\sin^2\theta}.$$

It follows from (8), (10) that in extreme cases, $u_y(\tau)$, $p(\theta)$ functions at high $\tau > 1/\varepsilon_0$ times contain oscillations only at the first harmonic (if further expanded — at odd harmonics). $X(\tau)$, $\Gamma(\theta)$ functions contain oscillation only at the second and the zeroth harmonics (if further expanded — at even harmonics).

Numerical solution at arbitrary a_0, ε_0 demonstrates both velocity oscillations u_y, $\dot{X}$ at laser harmonics and emergence of new combined frequencies. A characteristic numerical (MCAD) solution to (6) at $\varepsilon_0 = 6$, $a_0 = 9$ is shown in Fig. 2. It can be seen at Fig. 2 that under the action of a pulse with a steep leading edge, first the transverse oscillations of electron layer arise followed by longitudinal oscillations. Velocities of these oscillations achieve relativistic values as early as during first cycles of the laser pulse. At the pulse maximum the oscillations are nonlinear, aperiodic, contain high-frequency harmonics. After the end of pulse the longitudinal oscillations are continued (system (6) has no dissipative terms).

Calculations at the same laser intensity ($a_0 = 9$) and a thinner ($\varepsilon_0 = 9$) target, as well as at a thicker target, demonstrate a resonant dependence of longitudinal oscillation

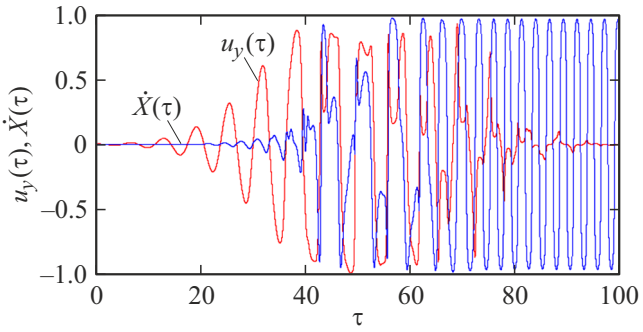

Figure 2. Longitudinal $\dot{X}(\tau)$ (blue curve) and transverse $u_y(\tau)$ (red curve) velocities of the electron layer for the following parameters of target and laser pulse: $\varepsilon_0 = 6$; $a_0 = 9$. Pulse duration is 12 cycles.

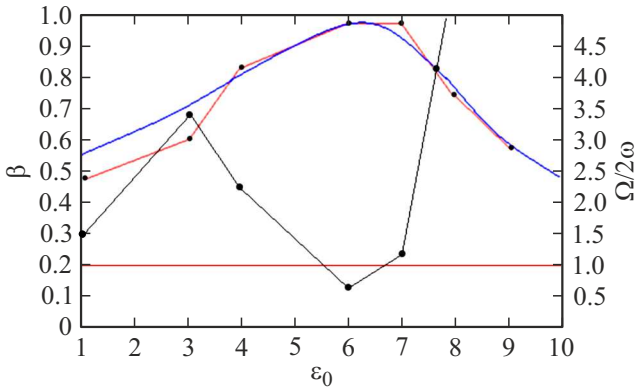

Figure 3. Dependence of maximum velocity $\beta(\varepsilon_0; a_0 = 9)$ of longitudinal oscillation of a thin target (velocity is directed backward) on the target thickness ε_0. Red polyline — numerical (MCAD) solution to (6), blue line — approximation by equation (12). Black polyline — dependence of frequency ratio $\Omega_U/2\omega$ (between the frequency of electron oscillation in the field of ion core and the frequency of ponderomotive force) on ε_0 at $a_0 = 9$. Red horizontal line corresponds to the case of frequency coincidence — a resonance of ponderomotive and ambipolar forces.

maximum velocity on the parameter of ε_0: maximum values of $\dot{X}(\tau)$ at $\varepsilon_0 = 1$ and at $\varepsilon_0 = 9$ are less than those shown in Fig. 2 at $\varepsilon_0 = 6$. It is shown below that the duration and spectrum of the attopulse are defined by the maximum velocity of longitudinal oscillations in the backward direction $\dot{X}_{\max} = \beta(a_0, \varepsilon_0)$.

For a single electron $\beta(a_0, \varepsilon_0 = 0) = a_0^2/(2 + a_0^2)$, its velocity is directed forward (10). Maximum of the $\beta(a_0, \varepsilon_0)$ function is related to the nonlinear resonance of longitudinal forces acting on the electron layer. The motion law $X(\tau)$ and the longitudinal velocity $\dot{X}(\tau)$ are defined by the second equation of systems (2), (6). This equation at high oscillation amplitudes, $|X(\tau)| > \omega l_f/2c$, describes electron oscillation in a potential field $U(x) = 2\pi e^2 n_e l_f |x|$ of a thin ion core (term $\sim f_{\text{am}}$ in (2)) under the action of ponderomotive pressure force $u_y \frac{\partial a_y^{(\text{ext})}(X(\tau),\tau)}{\partial X(\tau)}$, oscillating at a frequency of 2ω. When there is no laser field ($a_y^{(\text{ext})} = 0$, $u_y = 0$), the second equation in systems (2), (6) describes relativistic nonlinear oscillation in the potential of $U(x) = 2ie^2 n_e l_f |x|$.

From (6) at $a_y^{(\text{ext})} = 0$, $u_y = 0$ it is easy to find frequency of these oscillations as a function of maximum velocity $\beta(a_0, \varepsilon_0)$:

$$\Omega_U(a_0, \varepsilon_0) = \frac{\pi}{2}\varepsilon_0\omega\sqrt{\frac{1-\beta^2(a_0,\varepsilon_0)}{\beta^2(a_0,\varepsilon_0)}}. \qquad (11)$$

Note that with decrease in oscillation amplitude, $|X(\tau)| < \omega l_f/2c$, frequency (11) becomes the frequency of plasma oscillations $\Omega_U \to \Omega$. The red polyline in Fig. 3 shows dependence of $\beta(\varepsilon_0)$, that follows from the numerical solution to system (6) at $a_0 = 9$. It can be seen that at $\varepsilon_0 \sim 6-7$ there is a local maximum of longitudinal oscillation velocity of the electron layer. Black polyline and red horizontal line in Fig. 3 show that the range of $\varepsilon_0 \sim 6-7$ corresponds to the coincidence of frequencies, i.e. a nonlinear resonance ($\Omega_U \approx 2\omega$) between two forces in the second equation of system (6). Thus, at low ($\varepsilon_0 \ll 1$) and high ε_0 the law of electron motion contains oscillations with significantly different frequencies, $\Omega_U \ll 2\omega$ and $\Omega_U \gg 2\omega$. These frequencies become equal at the resonance. To achieve maximum conversion of laser pulse into attopulse, maximum amplitudes of the velocity of electron longitudinal oscillation are needed $\dot{X}_{\max} \to 1$, i.e. the case of resonance is optimum. The fundamental harmonic of oscillation at the resonance has a frequency of 2ω, while the oscillation of transverse velocity $u_y(\tau)$, in accordance with (6) has a frequency of ω.

Thus, the main regularities of the attopulse spectrum should be reproduced for the law of electron layer motion (solution to system (5)):

$$X(\tau) = X_0 + \frac{\beta(a_0, \varepsilon_0)}{2}\sin 2\tau, \quad \beta \to 1,$$

$$u_y(\tau) = u_{0y}\sin(\tau + \delta), \quad u_{0y} = \sqrt{1 - \beta^2 + (\pi/2 - \delta)^2},$$

$$\beta(a_0, \varepsilon_0) = \frac{(\varepsilon_0^2 + 1)a_0^2}{2 + (\varepsilon_0^2 + 1)a_0^2 + 0.4\varepsilon_0^4 a_0}. \qquad (12)$$

The analytical expression for $\beta(a_0, \varepsilon_0)$ is shown in Fig. 3. It should be emphasized that (12) is not a rigorous solution to initial equations (6), but just qualitatively corresponds it if maximum velocity $\beta(a_0, \varepsilon_0)$ of longitudinal oscillation coincides with numerical solution to (6) (blue and red curves in Fig. 3). In particular, there are no high-frequency harmonics of longitudinal and transverse velocities in (12), that can be seen in Fig. 2. However, the high-frequency harmonics of fields (1) are not lost, because velocities in (12) are ultrarelativistic.

By using (12) to obtain Fourier spectrum of the E_y component of electric field (1) (the magnetic field differs

only in sign and has the same spectrum):

$$\frac{eE_y(X,\sigma)}{mc} = -\varepsilon_0 \int\limits_{-\infty}^{\infty} u_y(\tau) e^{i\frac{\varpi}{\omega}(\tau+|X-X(\tau)|)} d\tau, \qquad (13)$$

the spectral energy distribution per unit area can be calculated:

$$\frac{d\varepsilon}{d\varpi} = c|E_y(x,\varpi)|^2. \qquad (14)$$

As can be seen from (13), X coordinate is not included in spectrum (14). However, the spectrum is dependent in the sign of X (face and rear sides of the target). At integer $n = \varpi$ formula (14) yields intensity of the n-th harmonic of the laser radiation.

By substituting (12) in (13), (14), we obtain an analytical formula for the spectrum of attopulse energy:

$$\frac{d\varepsilon}{d\varpi} = \frac{c(en_e l_f)^2}{\omega^2} u_{oy}^2 \left(\cos^2\delta \left[J_{\frac{n-1}{2}}\left(\frac{n\beta}{2}\right) - J_{\frac{n+1}{2}}\left(\frac{n\beta}{2}\right)\right]^2 \right.$$
$$\left. + \sin^2\delta \left[J_{\frac{n-1}{2}}\left(\frac{n\beta}{2}\right) + J_{\frac{n+1}{2}}\left(\frac{n\beta}{2}\right)\right]^2 \right), \quad n = \varpi/\omega. \qquad (15)$$

Dimensionless spectrum (15)

$$P(n) = \left(\frac{d\varepsilon}{d\varpi}\right) \Big/ \left(\frac{c(en_e l_f)^2}{\omega^2} u_{oy}^2\right)$$

at different $\beta(a_0\varepsilon_0)$ is shown in Fig. 4. Comparison of the analytical spectrum obtained by formulae (15), (12) with the analytical spectrum obtained by substituting to general formulae (13), (14) the laws of target motion $X(\tau)$, $u_y(\tau)$ obtained by numerical (using MCAD) integration of system (6), has shown that approximation (12) is sufficient to calculate the spectrum of radiation in the region of resonance between ponderomotive and ambipolar forces. Also, formula (15) is matched well with the spectrum of radiation obtained at the same parameters by numerical 1D-modelling using the LPIC code. Thus, the approximations made to derive motion equations (6) and „solutions" (12) to them are correct and the obtained spectra correspond to the spectra of numerical calculations. Note that analytical (15) and numerical spectra of target radiation contain the zeroth harmonic $n = 0$. It means the unipolarity (the presence of an other than zero time-averaged field component [16]) of the electromagnetic pulse reflected from and passed through the target. The unipolar ($n = 0$) component has a time duration in the order of the laser pulse length and does not contribute to the attosecond pulse. Also, note that $P(n = 0) \to \infty$, which is related to the infinite interval of integration over time in (13). When integrating the action of laser pulse over time, value of $P(n = 0)$ is finite. For other harmonics $P(n)$ is independent on the length of laser pulse at large number of its cycles.

Let us derive a high-frequency asymptotics (15) at $n \to \infty$, $\delta = 0$. For this purpose, we need to use the

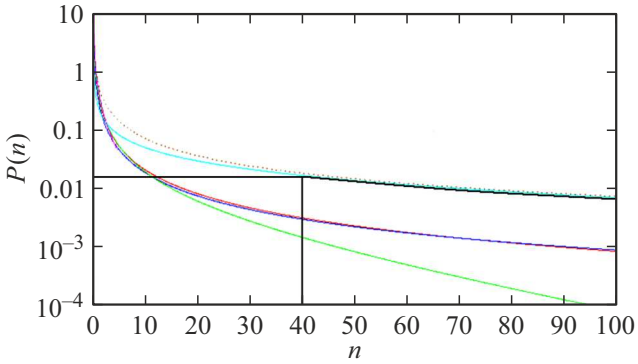

Figure 4. Analytical spectrum taking into account only fundamental harmonics in motion laws at different maximum velocities. Lightcyan line $\beta = 0.98$, $\delta = \pi/2$, dotted line — asymptotics of $P(n) \approx 0.72/n$. Red line $\beta = 0.98$, $\delta = 0$, blue line — asymptotics of $P(n) \approx 0.4n^{-4/3}$. Green line $\beta = 0.9$, $\delta = 0$, n — harmonic number, ordinate scale is in units of $P(n) = (d\varepsilon/d\varpi)/(c(en_e I_f)^2 u_{oy}^2/\omega^2)$.

asymptotics of Bessel functions at $n \gg 1$:

$$J_{\frac{n-1}{2}}\left(\frac{n\beta}{2}\right) = J_{\frac{n-1}{2}}\left(\frac{(n-1)}{2}\beta\left(1+\frac{1}{n-1}\right)\right) \xrightarrow[n\gg 1]{}$$
$$\xrightarrow[n\gg 1]{} \frac{1}{\sqrt{\pi}}\left(\frac{4}{n-1}\right)^{1/3} Ai\left(\left(\frac{n-1}{4}\right)^{2/3}\left(1-\beta^2\left(1+\frac{1}{n-1}\right)^2\right)\right). \qquad (16)$$

At high arguments of two Airy functions of asymptotics of $J_{\frac{n-1}{2}}$, $J_{\frac{n+1}{2}}$ are close to each other, therefore the difference of these functions in (15) is expanded in Taylor series. As a result, in the frequency interval of $n^{2/3}(1-\beta) \ll 1$ the difference is $(J_{\frac{n-1}{2}} - J_{\frac{n+1}{2}}) \sim n^{-2/3}$, and expression (15) — $\sim n^{-4/3}$. At $n^{2/3}(1-\beta) > 1$ spectrum (15) exponentially decays with growth of n. Asymptotics of the spectrum $\sim \varpi^{-4/3}$ at $n^{2/3}(1-\beta) \ll 1$ and $\beta \to 1$ is in compliance with [8].

Asymptotics $0.4n^{-4/3}$ for spectrum (15) is shown in Fig. 4 with blue line. It can be seen that it describes spectrum (15) at $\beta \to 1$, $\delta = 0$. Comparison of Fig. 4 with results of numerical modelling by the LPIC code shows that formula (15) correctly describes the spectrum and its changes when approaching to the point of maximum conversion at $\delta = 0$. At the same time, the parameter of $\beta(a_0, \varepsilon)$ must be taken from solution to system (6). $\beta(a_0 = 0, \varepsilon_0)$ function is shown in Fig. 3. Note, that at $\delta = \pi/2$ the spectrum is more gently sloping (blue curve in Fig. 4) and has an asymptotics of $0.7n^{-1}$. However, the case of $\delta = \pi/2$ corresponds to thick targets and is not optimum in terms of conversion to attopulses.

The electric field E_y (squared absolute value) of attopulses in time domain (1), obtained by numerical solution (5) in the MCAD software program, has the profile shown in red in Fig. 5. Peaks of the red curve in Fig. 5 are the attopulses of the radiation reflected from the target. They follow one after another with a period close to half

of that of the laser pulse (the period of ponderomotive pressure force). The number of attopulses is equal to the double number of laser pulse periods (the ponderomotive force oscillates at a double laser frequency). It can be seen in Fig. 5 that the period of attopulses repetition is not a constant value: time interval between them varies. Maximum faults (changes) of the period take place at an optimum value of parameter ε_0, when runouts occur at nonlinear resonance between the ponderomotive pressure and the force of ambipolar field. The field of a single attopulse in zoomed-in scale is shown in the insert in Fig. 5 and has a characteristic length of $\tau_a \approx 2^{1/2}\pi(1-\beta)^{3/2}/\omega$, where $\beta(a_0, \varepsilon_0)$ is maximum velocity (forward and backward, in units of s) of the electron layer where the attopulses are considered. The evaluation of duration follows from spectrum asymptotics (16) and properties of the Airy function, which decreases exponentially if its argument $((n-1)/4)^{2/3}(1-\beta^2(1+1/(n-1))^2) > 1$. At $n = \varpi^*/\omega \gg 1$ and $\beta \approx 1$ frequency of „steep" spectrum is $\varpi^* \sim 2^{1/2}\omega/(1-\beta)^{3/2}$, which corresponds to the above-mentioned characteristic duration of attopulse. Amplitude of the attopulse field (peak height in Fig. 5) is $2\pi\sigma_e/(1-\beta(a_0, \varepsilon_0))$, which follows from formula (1). The results of numerical PIC-calculation shown in Fig. 5 as a black line, at the same parameters of laser and target, show that the thin target approximation is valid for several first cycles of the pulse. Then the attopulse in the LPIC-calculation disappears, while in the model it is still there. The analysis of electron density of target in the LPIC-calculation shows that the attopulse degradation takes place due to its spreading and transformation of the thin electron layer into a cloud of electrons. In other words, a little dispersion of initial coordinates of electrons (within the initial thickness of the target) due to fast divergence of phase trajectories of individual particles results in a significant (by ten folds) dispersion of electron coordinates after several cycles. Therefore, in the second half of an eight-cycle pulse the approximation of thin target model does not work, the spread target no longer generates the attopulses (Fig. 5), though high-frequency harmonics are still there in the spectrum of reflected radiation. By decreasing the length of pulse down to $\sim 4-5$ cycles, it is possible to avoid degradation of attopulse and increase the conversion ratio. As shown below, it is possible to increase the conversion ratio of a „long" (more than four cycles) pulse using several targets positioned in series.

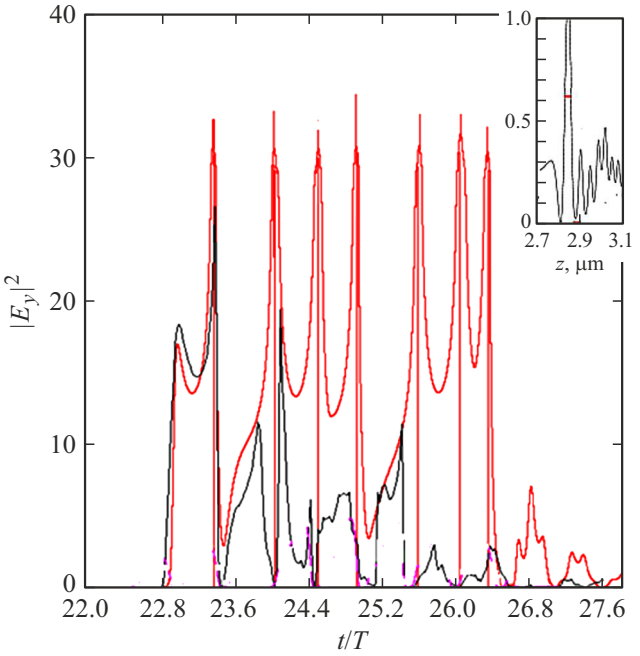

Figure 5. Squared absolute value of dimensionless $(eE_y/m_e\omega c)$ electric field (1) of attopulses in time domain for attopulses propagating backwards, at $a_0 = 9$, $\varepsilon_0 = 4$. The calculation is performed for $a_0 = 9$, $\varepsilon_0 = 4$ and a Gaussian incident pulse with a length of 8 cycles. Red color — model of thin target, black color — LPIC-calculation. The red section in the insert shows spatial length (in μm) of a single attopulse with an amplitude normalized to unity.

Conversion ratio of laser pulse into attopulse

Let us consider a sequence of attopulses with a Gaussian waveform and a given length τ_a (Fig. 5):

$$E_y(t) = \sum_{i=1}^{N} C_i \exp\left(-\frac{(t-t_i)^2}{\tau_a^2}\right), \quad \tau_a \ll t_i - t_{i-1}. \quad (17)$$

Fourier spectrum of such a sequence is as follows:

$$E_y(\varpi) = \tau_a\sqrt{\pi}\exp\left(-\frac{(\varpi\tau_a)^2}{4}\right)\sum_{i=1}^{N} C_i e^{i\varpi t_i}. \quad (18)$$

If attopulses have equal amplitude C and follow one after another with a regular period of T, the coefficient before the Gaussian exponent in (18) results only in modulation of the spectrum by harmonics of the period:

$$\sum_{i=1}^{N} C_i e^{i\varpi t_i} = C\,\frac{e^{i\varpi NT}-1}{e^{i\varpi T}-1}, \quad \left|C\,\frac{e^{i\varpi NT}-1}{e^{i\varpi T}-1}\right|^2$$

$$= |C|^2\,\frac{\sin^2 \varpi NT/2}{\sin^2 \varpi T/2} \to \pi N|C|^2\sum_{n=0}^{\infty}\delta(\varpi T/2 - n\pi). \quad (19)$$

The characteristic form (the steep of spectrum envelope at high frequencies) is defined only by the Gaussian exponent in the complete spectrum of attopulses:

$$\frac{d\varepsilon}{d\varpi} = c|E_y(\varpi)|^2$$

$$= c\pi^2 N|C|^2\tau_a^2\exp\left(-\frac{(\varpi\tau_a)^2}{2}\right)\sum_{n=0}^{\infty}\delta(\varpi T/2 - n\pi). \quad (20)$$

Integral of spectrum (20) over all frequencies (the energy of attopulses) is as follows:

$$\sum_{n=0}^{\infty} c\pi^2 N|C|^2\tau_a^2 \exp\left(-\frac{(2\pi n\tau_a/T)^2}{2}\right)$$

$$= c\pi N|C|^2\tau_a\sqrt{\pi/2} = c\pi^2 N|C|^2\tau_a^2\varpi^* \exp\left(-\frac{(\varpi^*\tau_a)^2}{2}\right)$$

$$= \varpi^2\frac{d\varepsilon}{d\varpi^*}, \quad \varpi^* = \frac{0.37}{\tau_a}\sqrt{\pi/2} \tag{21}$$

and equal to the area of a rectangle with a height of $\frac{d\varepsilon}{d\varpi^*}$ (we mean the spectrum envelope) and a width of ϖ^*, where $\varpi^* = \frac{0.37}{\tau_a}\sqrt{\pi/2}$. Let us determine the conversion ratio κ to attopulse as a ratio of energy (21) to the full energy of the laser pulse:

$$\kappa = \frac{\varpi^*\frac{d\varepsilon}{d\varpi^*}}{\sqrt{\pi}cE_0^2t_L/8\pi}$$

$$= \frac{8\pi^{1/2}\varepsilon_0^2\varpi^*}{a_0^2\omega t_L}\left|\int_{-\infty}^{\infty} u_y(\tau)e^{i\frac{\varpi^*}{\omega}(\tau+|X-X(\tau)|)}d\tau\right|^2, \tag{22}$$

where frequency $\varpi^* = \tau_a^{-1}\sqrt{\pi/2}$. Ratio (22) demonstrates maximum for ε_0, and for normal incidence it has a value comparable with the conversion ratio [7], which is introduced by another way: it is the energy of all frequencies starting from the given lower limit frequency of attopulse ϖ^*:

$$\kappa_R = \frac{\int_{\varpi^*}^{\infty}\frac{d\varepsilon}{d\varpi}d\varpi}{\sqrt{\pi}cE_0^2t_L/8\pi} = \frac{8\pi^{1/2}\varepsilon_0^2}{a_0^2\omega t_L}\int_{\varpi^*/\omega}^{\omega} d(\varpi/\omega)$$

$$\times\left|\int_{-\infty}^{\infty} u_y(\tau)e^{i\frac{\varpi}{\omega}(\tau+|X-X(\tau)|)}d\tau\right|^2. \tag{23}$$

Both ratios (22), (23) can be determined either analytically, using motion equation (6), or using the numerically obtained (PIC-modelling) spectra of the secondary radiation. On the basis of spectrum (15), at $\delta = 0$ an analytical formula can be presented for the conversion ratio we use:

$$\kappa(a_0, \varepsilon_0) =$$

$$= \frac{\frac{c(en_el_f)^2}{\omega^2}u_{oy}^2 n^*\left[J_{\frac{n^*-1}{2}}\left(\frac{n^*\beta(a_0,\varepsilon_0)}{2}\right) - J_{\frac{n^*+1}{2}}\left(\frac{n^*\beta(a_0,\varepsilon_0)}{2}\right)\right]^2}{\sqrt{\pi}cE_0^2t_L/8\pi}, \tag{24}$$

$$n^* = (\tau_a\omega)^{-1}\sqrt{\pi/2},$$

$$\beta(a_0, \varepsilon_0) = \frac{(\varepsilon_0^2+1)a_0^2}{2+(\varepsilon_0^2+1)a_0^2+0.4\varepsilon_0^4a_0^1}.$$

Geometrically ratio (22) is an area of a rectangle (highlighted with black color in Fig. 4), and ratio (23) is an area under the spectrum „tail“ (also highlighted with black color in Fig. 4), normalized to the full energy of laser pulse.

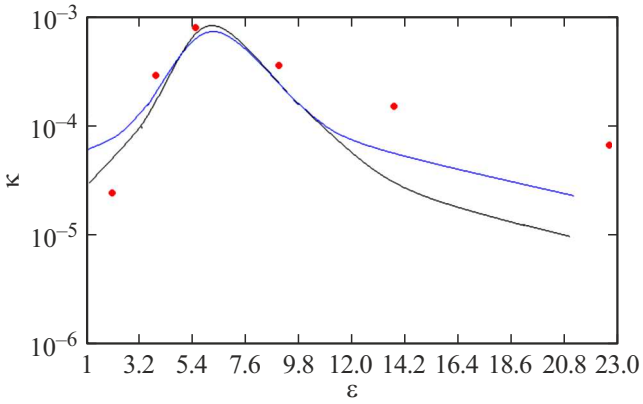

Figure 6. „Backward“ conversion ratio as a function of parameter ε_0. Orange circles — 1D-calculation at $a_0 = 9$. Black line — formula (24), blue line — formula (22) and MCAD-calculation for functions of $X(\tau)$, $u_y(\tau)$.

The black rectangle in Fig. 4 shows conversion ratio (22) to attopulse of the 40-th harmonic ($\tau_a = 2\pi/40\omega$). Value of conversion ratio in Fig. 4 is $\kappa \approx 10^{-3}$. Conversion ratio (23) to the spectrum „tail“ higher than the 40-th harmonic is $\kappa_R \approx 7\cdot 10^{-4}$ in this case. Thus, different definitions (22), (23) of the conversion ratio yield values comparable in order of magnitude. In our view, definition (22) in a greater degree meets the physical meaning, i.e. extraction of the attopulse spectrum („rectangular“ in Fig. 4) in the general spectrum of reflected and passed through radiation.

Ratio (22) can be considered separately in front of the target (backward reflected attopulses) and behind the target (passed through attopulses). At a given laser intensity (parameter a_0) ratio (22) has a maximum over ε_0 with fixed values of other parameters of the problem. The maximum conversion corresponds to the nonlinear resonance in motion equations (6) of the analytical model.

Note, that ratio (23) introduced in [7] defined the conversion into the hard part of the spectrum, however the spectrum itself can be not corresponding to an attopulse. For example, in thick targets conversion ratio (23) can be significant, but the field of harmonics does not put together into an attopulse, but is a saw-tooth oscillation, which high-frequency part is related to large slope angle of the saw „teef“.

Figure 6 shows the dependence of conversion ratio into the backward reflected attopulse on ε_0 determined by formula (24) for $a_0 = 9$, $\varpi^*/\omega = 40$ and a laser pulse with rectangular time profile of 12 cycles. Maximum conversion ratio as calculated by formula (24) at $a_0 = 9$ is $8\cdot 10^{-4}$. Note, that in the radiation passed through the target the ratio of conversion into attopulse is as low as $2.3\cdot 10^{-5}$ (the formula for conversion ratio into passed through attopulse is obtained by the $\tau + |X - X(\tau)| \to \tau - |X - X(\tau)|$ re-

placement in the exponent power in (22)). To verify the obtained results at the same parameters of the laser pulse, 1D-calculations by the LPIC code [17] were performed with different values of ε_0, and the result of these calculations is shown in Fig. 6 as well (orange circles).

It can be seen from Fig. 6 that the model reproduces 1D-calculations to determine values of optimum ε_0 to achieve maximum conversion into the attopulse spectrum. The maximum amplitude of the attopulse spectrum for $a_0 = 0$ is realized at $\varepsilon_0 \sim 6$ with little changes of ε_0 parameter ($9 \to 6 \to 4$) needed in the model to pass over the conversion maximum. Note, that the maximum conversion ratio over the target thickness was obtained numerically in [9,10] using EPOCH PIC-code. In calculations of [10], maximum conversion corresponded to the dimensionless parameter of $n_e d/n_{cr}\lambda a_0 = 0.2$. In the maximum in Fig. 6 this parameter $n_e d/n_{cr}\lambda a_0 = \varepsilon_0/\pi a_0 = 6/9\pi \approx 0.2$. Thus, the built-up model (22) for the conversion ratio corresponds to 1D PIC-calculations of [9,10].

The 1D-calculation and model (6), (22) in the region of optimum ε_0 yield a significant (by order of magnitude) exceedance of the „backward" conversion ratio over the „forward"conversion ratio. This is related to a greater speed of electron layer oscillation in the case of backward motion as compared to the forward motion, and suppression of the forward-generated attopulse, respectively. Note, that in the numerical modelling of [18], the backward reflected attopulse also had a greater intensity and a lower duration. Also, it should be noted that approximation (12) of solutions to system (6) does not take into account the difference between „forward-backward" oscillations and can not be used to calculate parameters of the passed-through attopulse (numerical integration of (6) is needed).

The number of hard quanta in the attopulse can be evaluated as

$$N_\gamma \approx \frac{\kappa\varepsilon_L(1-\beta^2)^{3/2}}{\hbar\omega} = N_L\kappa(1-\beta^2)^{3/2}. \qquad (25)$$

As can be seen from (25), the conversion ratio over number of quanta N_γ/N_L differs from the conversion ratio over energy by the factor of $(1-\beta^2)^{3/2}$. The investigation of $\kappa(\varepsilon_0)(1-\beta^2(\varepsilon_0))^{3/2}$ function shows that its maximum is located at the same value of ε_0 as maximum of $\kappa(\varepsilon_0)$, $\beta(\varepsilon_0)$ functions, and the dependence of $N_\gamma(\varepsilon_0)$ has a profile similar to that shown in Fig. 6.

2D PIC-calculation of attopulse

For thin (tens of nanometers) targets the one-dimensional approximation is performed well, because the ratio between target thickness and laser beam diameter is very low. To illustrate correctness of the 1D-calculation, a 2D-calculation by the code [19] was performed. Parameters of the 2D-calculation are the same as in the 1D-calculation: $a_0 = 9$, $\varepsilon_0 = 4$. Diameter of the laser spot $d_L = 3.2\,\mu$m (4 wavelengths), pulse duration is 33 fs. Figure 7, *a* shows square of the field strength (intensity) of the reflected and passed through waves for five thin targets (shown with figures) and contribution of the first target to the field of the reflected pulse is highlighted separately with red color. First reflected cycles from each target (marked with figures corresponding to targets) form attopulses and are described by the thin layer model presented above. The coefficient of reflection of subsequent cycles of the laser pulse from each target decreases with time (due to expansion of the electron density), therefore the „tail" of the pulse is weakly reflected from each target. However, the use of several targets allows the entire pulse length to be involved and increases the resulted conversion ratio. Due to absorption and reflection of the laser pulse by each target the amplitude of attopulses decreases with increase in number of the target. As a result, the attopulses numbered in accordance with targets in Fig. 7, *a* are arranged in a row by decreasing amplitude. Figure 7, *a* shows that an amplitude filter (that does not change pulse duration) makes it possible to separate several (according to the cut-off level) attopulses from the whole reflected train. The spatial duration of an individual attopulse in Fig. 7, *a* is ~ 40 nm, that is shown in Fig. 7, *b*, which is a fragment of Fig. 7, *a* with zoomed resolution. If attopulse amplitudes are cut off at a level of 0.5 of the laser amplitude, then the ratio of conversion into energy of attopulses for five targets in Fig. 7, *a* reaches ~ 0.01, which is an order of magnitude higher than the conversion ratio of a single target. Figure 8 shows 2D-distribution of field of the attopulse reflected from a single target (highlighted with red color in Fig. 7, *a*). A 2D-effect (which is absent in the consideration presented above) is the curving of the attopulse front edge and emergence of angular divergence. In formula (12) the offset $X(\tau)$ of the target electron density is found at oscillation under the action of ponderomotive pressure force. In dimension units the amplitude of this offset is: $\Delta x = c\beta(a_0, \varepsilon_0)/2\omega = \beta(a_0, \varepsilon_0)\lambda_L/4\pi$. Appropriately, the characteristic angle of attopulse divergence θ_{atto} is:

$$\theta_{\text{atto}} \approx \text{arctg}\,(\beta(a_0, \varepsilon_0)\lambda_L/2\pi d_L). \qquad (26)$$

The presented evaluation is valid for a flat front of the laser pulse incident on the target (the target is positioned exactly in the focus of the optical system). Curvature of the incident pulse front is added to evaluation (26) and increase or decrease the divergence depending on sign. For the experimental investigation of the attopulse, the backward reflection to the optical system of the laser is inconvenient, and it is reasonable to direct the attopulse along other directions. Figure 9, *a* shows that a small tilt of the target has a little effect on parameters of the attopulse, but allows directing it at another angles. To improve the conversion ratio, in Fig. 9, *a* a generation of attopulse from two tilted (with a tilt angle of 22.5°) targets spaced by a distance of $2\,\mu$m was considered. It can be seen that two „parallel" attopulses are formed. Thus, by applying several targets positioned at different angles, it is possible to separate

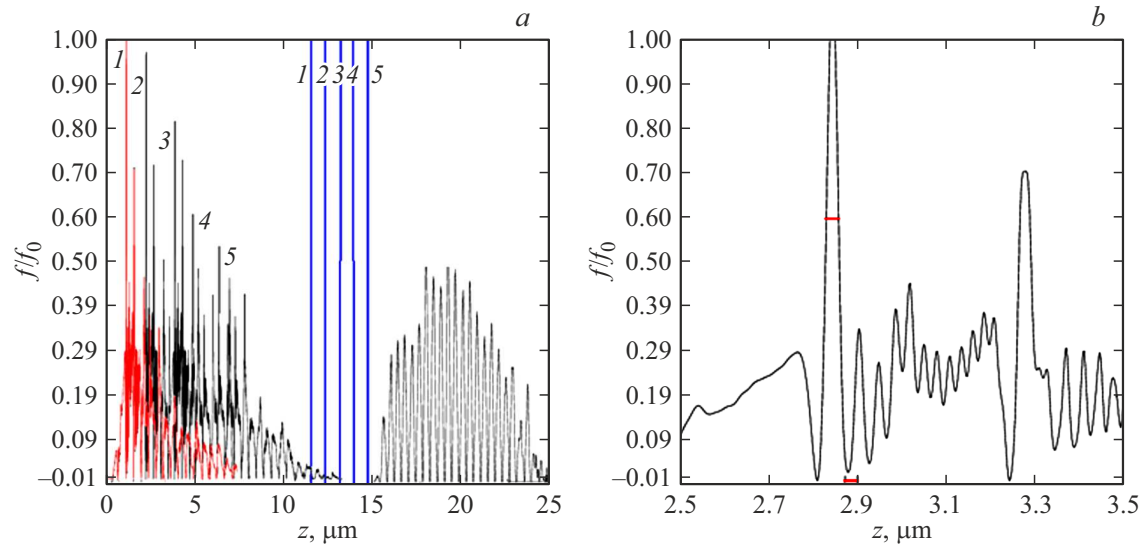

Figure 7. (*a*) Attopulses (square of the electric field strength) from five thin targets positioned in series. Attopulse of the first target is highlighted with red color on the general background. Blue color shows positions of five targets. (*b*) Attopulse of the first target is in zoomed spatial resolution. Spatial duration (red horizontal section) of the reflected attopulse ~ 40 nm, that has passed ~ 70 nm. Ordinate scale — in units of amplitude of the incident pulse.

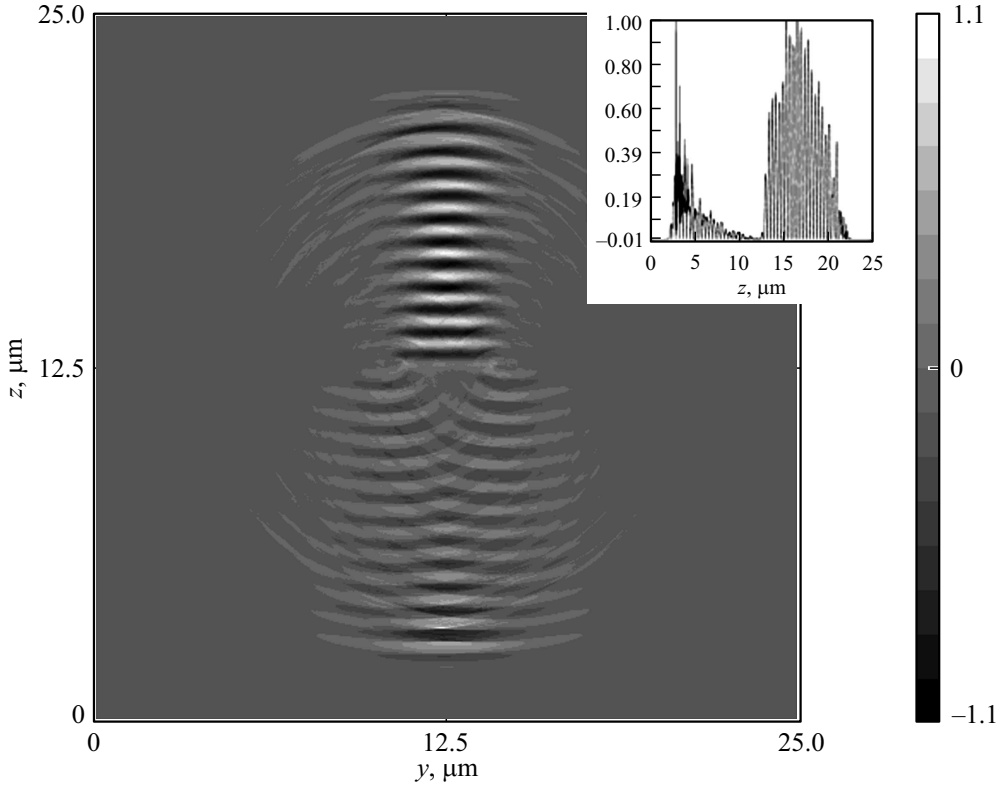

Figure 8. 2D-distribution of electric field of attopulse. Scale in units of incident laser field. The insert shows 1D-section of intensity over the axis of laser beam ($y = 12.5\,\mu$m). Parameters of 2D-calculation: $a_0 = 9$, $\varepsilon_0 = 4$, $d_L = 3.2\,\mu$m, $\tau_L = 33$ fs. The target is located at $z = 12.5\,\mu$m.

the attopulse into individual parts, shifted by defined time intervals, and direct them at different angles. The diffraction of radiation to directions other than the mirror direction in Fig. 9, *a* (spherical waves) is related to the edge-effects at the edges of the laser spot. Figure 9, *b* shows distribution of the electron charge density (scale in units of critical density) at the moment of time of 26 fs from the beginning of the laser pulse of 33 fs. At the edges of the laser spot a local

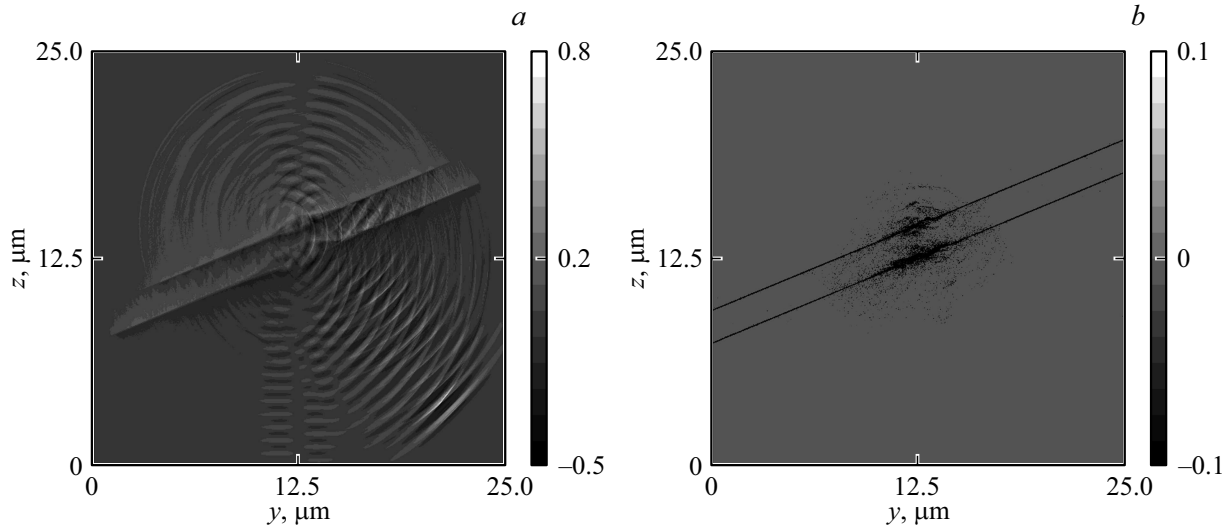

Figure 9. (*a*) 2D-distribution of electric field of the attopulse from two tilted (angle 22.5°) targets spaced by 2μm. Scale in units of incident laser field. (*b*) Electron charge density (scale in units of critical density) at the moment of time of 26 fs from the beginning of the laser pulse of 33 fs. Other parameters of the 2D-calculation are shown in Fig. 8.

curving and a modulation of the electron density can be seen, that resulted in Fig. 9, *a* in a scattering of waves to directions other than the mirror direction. Note, that a 2D PIC-calculation of the conversion ratio into attopulse as compared with 1D PIC-calculation was carried out in [9]. It was shown that two-dimensional effects do not change values of parameters of target and laser pulse, which are optimum for the maximum conversion at a laser pulse diameter of several micrometers.

Conclusions

We investigated the spectrum of coherent secondary radiation (train of attopulses) arising as a result of interaction of a relativistic-intensity laser pulse with a thin (in the order of thickness of the skin-layer) solid target. Both the reflected radiation and the passed through the target secondary radiation are considered, including low (units of laser frequency) harmonics. It is shown that the secondary radiation is generated by relativistic electrons moving under the action of transverse field (incident and reflected laser pulses) and longitudinal field of the ion core of the thin target having a form of effective potential well for electrons. With a dimensionless amplitude $a_0 > 1$ of the laser field and a dimensionless thickness $\varepsilon_0 \approx 0.7a_0$ of the target (partially transparent target) a coincidence takes place between frequencies (resonance) of the electron oscillation under the action of oscillating (at a frequency of $2\omega_L$) ponderomotive pressure of the laser pulse and nonlinear oscillations of relativistic electrons in the potential well of the ion core of the thin target. The case of resonance is an optimum for the generation of maximum intensity secondary radiation with a maximum energy of X-ray quantum and a minimum length of attopulse, respectively. The efficiency of attopulse generation in conditions of resonance is comparable with or supersedes that for gas targets [20]. In previous studies [8,18] the attopulse generation by solid targets was investigated in a region far from the resonance, because non-transparent targets were considered with a large (as compared with the skin-layer) thickness.

The secondary (reflected and passed through) radiation contains narrow and high peaks (the attopulses) and a smoother part — the substrate. The attopulses can be separated from the substrate by an amplitude filter (similar to a plasma mirror that improves contrast). In the region of resonance in this study we have derived a formula for optimum thickness of the target as a function of the incident intensity and a scaling formula for the ratio of laser pulse energy conversion into the energy of attopulses. The conversion ratio to attopulses in this study is defined as a ratio between the area of attopulse radiation spectrum (a rectangular profile with a spectrum width of $\sim \tau_a^{-1}$) and the area of full radiation spectrum. This definition is different from the conversion ratio in [7], defined as a ratio between the energy in the exponential „tail“ ($\omega > \tau_a^{-1}$) of the secondary radiation spectrum and the energy of laser pulse. However, the ratio in [7] only defines the relative intensity of high-frequency harmonics of the spectrum which do not necessarily form an attopulse in the space-time domain. Our definition of conversion ratio makes it possible a more precise than in [7,8] determining of the ratio of a laser pulse conversion into a train of attopulses of a given duration. Maximum conversion ratio for a single target is determined ($\sim 10^{-3}$) and the possibility of its improvement up to ~ 0.1 using several successively positioned targets is shown. It is shown that in the optimum case the ratio of conversion to the attopulses propagating along the direction of the incident radiation is less than that into the attopulses of mirror

direction, which is related to the asymmetry (forward-backward) of target electron oscillations in the field of laser pulse and ion core. To verify the analytical calculations, 1D and 2D PIC-modelling of attopulse spectra and conversion ratio values was performed that confirmed the quantitative relationships of the considered model.

Conflict of interest

The authors declare that they have no conflict of interest.

References

[1] G. Sansone, L. Poletto, M. Nisoli. Nat. Photonics, **5**, 655 (2011).
[2] F. Krausz, M. Ivanov. Rev. Mod. Phys., **81**, 163 (2009). DOI: 10.1103/RevModPhys.81.163
[3] V.L. Ginzburg, V.N. Tsytovich. *Transition Radiation and Transition Scattering* (Nauka, M., 1984) 360 p.
[4] B. Dromey, S. Rykovanov, M. Yeung, R. Hörlein, D. Jung, D.C. Gautier, T. Dzelzainis, D. Kiefer, S. Palaniyppan, R. Shah, J. Schreiber, H. Ruhl, J.C. Fernandez, C.L. Lewis S., M. Zepf, B.M. Hegelich. Nature Phys., **8**, 804 (2012). DOI: 10.1063/1.5004641
[5] T. Baeva, S. Gordienko, A. Pukhov. Phys. Rev. E, **74**, 046404 (2006). DOI: 10.1103/PhysRevE.74.046404
[6] A.A. Andreev, S. Steinke, T. Sokollik, M. Schnürer, S.T. Avetsiyan, P.V. Nickles, K.Yu. Platonov. Phys. of Plasmas, **16**, 013103 (2009). DOI: 10.1063/1.3054528
[7] D. van der Brügge, A. Pukhov „Theory of Attosecond Pulses from Relativistic Surface Plasmas". Institut für theoretische Physik, Heinrich-Heine-Universit.t Düsseldorf. arXiv:1111.4133 (2011).
[8] D. van der Brügge, A. Pukhov. Phys. of Plasmas, **17**, 033110 (2010). DOI: 10.1063/1.3353050
[9] Yu.M. Mikhailova, V.T. Platonenko, S.G. Rykovanov. Pis?ma v ZhETF, **81**, 703 (2005) (in Russian).
[10] X. Xu, B. Qiao, T. Yu, Y. Yin, H. Zhuo, K. Liu, D. Xie, D. Zou, W. Wang. New J. Phys., **21**, 103013 (2019). DOI: 10.1063/1.5118805
[11] M.R. Edwards, J.F. Nathaniel, J.M. Mikhailova. Phys. Plasmas, **28**, 013105 (2021). DOI: 10.1063/5.0031459
[12] R. Lichters, Vehn J. Meyerter, A. Pukhov. Phys. Plasmas, **3**, 3425 (1996). DOI: 10.1063/1.871619
[13] V.A. Vshivkov, N.M. Naumova, F. Pegoraro, S.V. Bulanov. Phys. Plasmas, **5**, 2727 (1998). DOI: 10.1063/1.872961
[14] V.V. Kulagin, V.A. Cherepenin, H. Suk. Phys. Plasmas, **11**, 5239 (2004). DOI: 10.1063/1.1798471
[15] A.A. Andreev, K.Yu. Platonov, V.I. Chestnov, A.E. Petrov. Opt. i spektr., **117**, 287 (2014) (in Russian).
[16] N.N. Rozanov, M.V. Arkhipov, R.M. Arkhipov. UFN, **188**, 1347 (2018) (in Russian). DOI: 10.3367/UFNr.2018.07.038386
[17] R.E.W. Pfund, R. Lichters, J. Meyer-ter-Vehn. AIP Conference Proceedings, **426**, 141 (1998). DOI: 10.1063/1.55199
[18] M. Yeung, B. Dromey, D. Adams, S. Cousens, R. Hörlein, Y. Nomura, G.D. Tsakiris, M. Zepf. PRL, **110**, 165002 (2013). DOI: 10.1103/PhysRevLett.110.165002
[19] A. Kemp, H. Ruhl. Phys. of Plasmas, **12**, 033105 (2005). DOI: 10.1063/1.1856933
[20] V.V. Strelkov, V.T. Platonenko, A.F. Sterzhantov, M.Yu. Ryabikin. UFN, **186**, 449 (2016) (in Russian). DOI: 10.3367/UFNr.2015.12.037670